Phase coexistence and magnetic anisotropy in $La_{1-x}Ca_xMnO_3$ ($0<x\leqslant 0.23$) studied via electron spin resonance

V. Likodimos and M. Pissas
Institute of Materials Science, NCSR, Demokritos, 153 10 Aghia Paraskevi, Athens, Greece
(Received 26 January 2007; revised manuscript received 22 April 2007; published 18 July 2007)

We report an electron-spin-resonance (ESR) study of stoichiometric $La_{1-x}Ca_xMnO_3$ for $0<x\leqslant 0.23$. The room-temperature ESR linewidth shows a marked decrease with x that is mainly due to the variation of the magnetic susceptibility and a much slower evolution of spin relaxation, associated with the interplay of crystal-field and superexchange interactions. In the canted antiferromagnetic regime, the ESR parameters show initially an x-dependent ferromagnetic (FM) behavior that evolves to antiferromagnetic in the vicinity of T_N, reflecting the development of spin canting. A weak ferromagnetic-resonance (FMR) mode is observed below T_N that becomes enhanced near the phase boundary to the ferromagnetic insulating (FMI) phase. This mode persists at higher doping levels ($x\leqslant 0.16$) and is attributed to residual FM domains due to the release of crystal strain near the structural transformation at $T<100$ K. In the FMI regime, FMR measurements show strong uniaxial magnetic anisotropy up to $x=0.16$ with $K=(1-2)\times 10^6$ erg/cm^3 at 100 K. The temperature dependence of the magnetic anisotropy reveals power-law scaling with the magnetization, $K(T)\propto M(T)^3$, indicative of single-ion magnetocrystalline anisotropy and the persistence of orbital order in the FMI state. As the FM metallic phase is approached, the magnetic anisotropy decreases significantly and an additional FMR mode systematically emerges in the paramagnetic regime at $T\lesssim 260$ K for $x=0.19-0.23$. Its relative spectral weight grows with x indicating an increase of the underlying FM fraction that correlates with the enhanced metallic behavior.

DOI: 10.1103/PhysRevB.76.024422 PACS number(s): 75.30.Gw, 75.47.Lx, 75.47.Gk, 76.50.+g

I. INTRODUCTION

Colossal magnetoresistive (CMR) manganites $R_{1-x}A_xMnO_3$ (R=lanthanide and A=alkaline-earth ions) have attracted tremendous interest among the strongly correlated electron systems due to their unique physical properties, stemming from the close interplay of spin, charge, orbital, and lattice degrees of freedom.[1] Extensive research efforts have shown that depending on the doping concentration x and the average ionic radius of the A cation site that control the band filling and the e_g electron transfer or the one-electron bandwidth, respectively, competition between the double exchange[2] (DE) with the Jahn-Teller coupling, charge and/or orbital order, and superexchange (SE) interactions leads to complicated phase diagrams with strong tendencies toward phase separation at different length scales and intriguing magnetoresistive and magnetostructural phenomena.[3–7] A common feature shared by most CMR manganites that is still poorly understood is the appearance at relatively low doping levels ($0.1<x<0.3$) of a ferromagnetic insulating (FMI) phase preceding the localized-to-itinerant transition to the ferromagnetic metallic (FMM) state, where ferromagnetism is mainly stabilized through the DE mechanism that maximizes the kinetic energy of e_g electrons via the strong on-site Hund coupling. Orbital and/or charge order, as well as phase separation into ferromagnetic (FM) and antiferromagnetic (AFM) phases and charge segregation, have been considered to explain this intriguing state.[8–10]

In particular, the parent $LaMnO_3$ compound undergoes a cooperative Jahn-Teller (JT) transition at $T_{JT}\approx 750$ K that stabilizes the long-range antiferrodistortive ordering of the e_g orbitals,[11] though local JT distortions have been recently found to persist at the length scale of 16 Å even at $T>T_{JT}$.[12] This orbital order leads to the layered A-type antiferromagnetic (A-AFM) spin structure at $T_N\approx 140$ K,[13] through the anisotropic SE interactions, FM in the ac planes, and AFM along the b axis (*Pnma* notation).[14] Such anisotropic SE coupling was indeed found by neutron scattering,[15] in qualitative agreement with the Goodenough-Kanamori-Anderson rules,[16] and theoretical predictions.[17,18] A major contribution from magnetocrystalline anisotropy, reflecting the orientation of the e_g orbitals, has also been predicted[17] and experimentally verified by neutron-scattering[15] and antiferromagnetic-resonance (AFMR) experiments[19–21] accounting for the easy magnetization axis and the weak canting of the Mn moments. Introduction of holes through A cation substitution in $LaMnO_3$ activates the DE interaction and the mobility of e_g electrons at neighboring $Mn^{3+,4+}$ sites. This has been originally proposed to result in the homogeneous canted antiferromagnetic (CAF) state,[2] though recent theoretical work shows that the CAF structure is unstable against phase separation into FM and AFM states.[6] Although magnetization and AFMR results in lightly doped $La_{1-x}Sr_xMnO_3$ are consistent with a homogeneous CAF state,[22–24] neutron-scattering experiments on both Ca- and Sr-doped manganites at $x\leqslant 0.1$ have shown an inhomogeneous ground state, namely, a spatially modulated AFM structure with FM droplets embedded in the CAF matrix.[25–28]

Upon further doping, the CAF phase evolves to the uncommon FMI phase in the range of $0.125\leqslant x<0.225$ for $La_{1-x}Ca_xMnO_3$, followed by the transition to the ferromagnetic metallic state at $x\approx 0.225$.[29–32] In the FMI regime, the cooperative JT effect weakens progressively with x and its long-range character becomes suppressed at the FMI-FMM boundary,[27,33,34] though short-range lattice distortions may

continue to exist in the FMM phase and correlate with the transport behavior.[35,36] For the large bandwidth $La_{1-x}Sr_xMnO_3$, the FMI phase is observed over a relatively narrow doping range close to $x=1/8$ $(0.10\leqslant x\leqslant 0.15)$, and its origin has been related to a new type of orbital ordering involving the formation of orbital polarons,[9,37] whereas the persistence of the staggered orbital order of the parent $PrMnO_3$ with reduced lattice distortions and SE anisotropy has been found in the narrow bandwidth $Pr_{0.75}Ca_{0.25}MnO_3$, where the FMI phase extends over the broad range of $0.15\leqslant x\leqslant 0.3$.[8,38] For the intermediate bandwidth $La_{1-x}Ca_xMnO_3$, an inhomogeneous FMI state has been proposed, consisting of "hole-rich" (Mn^{4+} rich) and "hole-poor" (containing mostly Mn^{3+}) orbitally ordered domains with anisotropic SE coupling constants that tend to become isotropic at the FMM state.[39]

High-resolution synchrotron x-ray experiments in stoichiometric $La_{1-x}Ca_xMnO_3$ $(0.11\leqslant x\leqslant 0.175)$ revealed that below T_{JT}, the crystal structure becomes monoclinic, with increasing crystal strain that reaches a maximum at T_C.[34] Below $T_{M'M''}\approx 60$ K, a structural transformation occurs to a less anisotropic structure involving a marked decrease of orthorhombicity and the release of the crystal strain, as well as distinct anomalies in the ac and dc magnetic responses and current-induced metastable resistivity,[31,34,40–42] where, according to NMR experiments, freezing to an inhomogeneous orbitally ordered state embodying metallic hole-rich walls has been suggested.[43,44] Very recently, ferromagnetic-resonance (FMR) experiments in $La_{1-x}Ca_xMnO_3$ $(0.125\leqslant x\leqslant 0.19)$ showed a strongly anisotropic FM phase with magnetic anisotropy that decreases considerably at $x=0.19$, close to the metallic phase boundary, as well as a tendency toward FM cluster formation in the paramagnetic regime for $x=0.175$ and 0.19.[45]

In this work, we present a detailed electron-spin-resonance (ESR) study of stoichiometric $La_{1-x}Ca_xMnO_3$ in order to probe the evolution of spin dynamics and phase coexistence in the compositional range of $0<x\leqslant 0.23$, extending from the orbitally ordered AFM phase of $LaMnO_3$ up to the FMM state. A strong reduction of the spin-relaxation rate with Ca doping is derived from the room-temperature ESR linewidth, related mostly to the increase of the magnetic susceptibility and to a lesser extent to the release of crystal strain and the decrease of the SE coupling anisotropy. The presence of local FM inhomogeneities is identified at Ca concentrations straddling the CAF-FMI phase boundary and most importantly at the localized-to-itinerant transition regime $(x=0.19-0.23)$, where an increasing fraction of FM clusters coexisting with the paramagnetic phase is systematically resolved above T_C. Temperature-dependent analysis of the magnetic anisotropy in the FMI regime reveals power-law scaling with the magnetization, suggestive of the magnetocrystalline origin of anisotropy and the persistence of orbital order in the precursor phase of the FMM state.

II. EXPERIMENTAL DETAILS

Stoichiometric $La_{1-x}Ca_xMnO_3$ samples with $0\leqslant x\leqslant 0.23$ were prepared following a particular solid-state reaction route with postannealing in He atmosphere in the final preparation stage, as previously described.[31] In contrast to "air prepared" samples, which are characterized by cation nonstoichiometry,[31,34,46–48] these postannealed samples exhibit all the features of the stoichiometric phase, especially the cooperative JT distortion. The samples have been thoroughly studied by high-resolution synchrotron x-ray and neutron-diffraction, ac and dc magnetometry, as well as resistivity measurements,[31,34] which reveal a systematic variation of their structural and magnetic properties with x, confirming the preparation of different samples with varying doping levels, even for the finest compositional step of $\delta x=0.005$. The unit-cell parameters match closely those reported by Dabrowski *et al.*,[47] for stoichiometric polycrystalline $La_{1-x}Ca_xMnO_3$ samples. Good agreement is also found with the phase diagram reported by Biotteau *et al.*[27] using single crystals, except for $x=0.1$. In that case, two successive magnetic transitions were resolved by both neutron-diffraction and magnetic-measurements,[27,49] a behavior that appears at $x=0.11-0.13$ for the present samples.

ESR measurements were performed with a Bruker ER 200D spectrometer at the X band ($\nu\approx 9.41$ GHz) using small amounts (1–5 mg) of fine powdered specimens either fixed in high-vacuum grease to avoid any texture in the FM state by the applied magnetic field or in loose packed form to improve spectral resolution through partial orientation by the magnetic field in the case of measurements above T_C.[50] The magnetic field was scaled with an NMR gaussmeter, while temperature-dependent measurements (4–300 K) were carried out employing an Oxford flow cryostat.

III. RESULTS AND DISCUSSION

For all doping concentrations $0\leqslant x\leqslant 0.23$, a symmetric exchange narrowed ESR line is observed at room temperature (RT). The resonance line can be accurately fitted to a single Lorentzian line shape provided that the resonance absorption at negative field due to the linearly polarized microwave field is taken into account.[51] A nearly constant g value at $g=1.99(1)$ is derived, independent of x. Figure 1(a) shows the x dependence of the peak-to-peak linewidth ΔH_{pp} that decreases appreciably with x, following closely the evolution of the $La_{1-x}Ca_xMnO_3$ phase diagram, shown for comparison in Fig. 1(b). Systematic ESR studies in the paramagnetic (PM) regime of both pure and lightly doped $LaMnO_3$ (Refs. 52–56) have shown that the ESR linewidth can be described by $\Delta H_{pp}=[\chi_0(T)/\chi(T)]\Delta H_0$, where $\chi_0=C/T$ is the free-ion susceptibility with C the Curie constant, $\chi(T)$ is the dc magnetic susceptibility of the coupled system, and ΔH_0 is determined by the contribution of anisotropic interactions to the exchange narrowed ESR linewidth, mainly due to the crystal-field (CF) interaction and the Dzyaloshinsky-Moriya antisymmetric exchange and their temperature dependence near the Jahn-Teller and the magnetic phase transitions. At temperatures well above T_C, T_N, and T_{JT}, the latter term can be identified as the high-temperature limit of ΔH_{pp}. To explore the variation of $\Delta H_{pp}(x)$, we have calculated the thermodynamic factor χ_0/χ using the Curie constant $C=N_A g^2\mu_B^2[xS_1(S_1+1)+(1-x)S_2(S_2+1)]=24-9x$ for

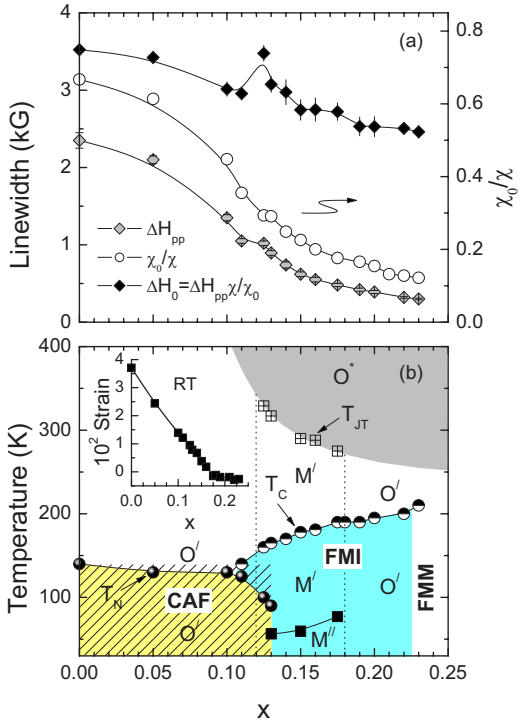

FIG. 1. (Color online) (a) ESR linewidth ΔH_{pp}, $\Delta H_0 = \Delta H_{pp}\chi/\chi_0$, and the ratio χ_0/χ as a function of x for $La_{1-x}Ca_xMnO_3$ at RT. (b) $T-x$ phase diagram ($0 \leqslant x \leqslant 0.23$) reconstructed from Refs. 31 and 34. The symbol O^* denotes orthorhombic *Pnma* symmetry with $c \geqslant a \geqslant b/\sqrt{2}$, $O^/$ corresponds to orthorhombic *Pnma* symmetry with $a > c > b/\sqrt{2}$, while $M^/$ ($M^{//}$) denote monoclinic $P2_1/c$ symmetry with $a > c > b/\sqrt{2}$ and strong (intermediate) anisotropic bond lengths. The inset shows the x variation of the orthorhombic unit-cell strain parameter $s=2(a-c)/(a+c)$.

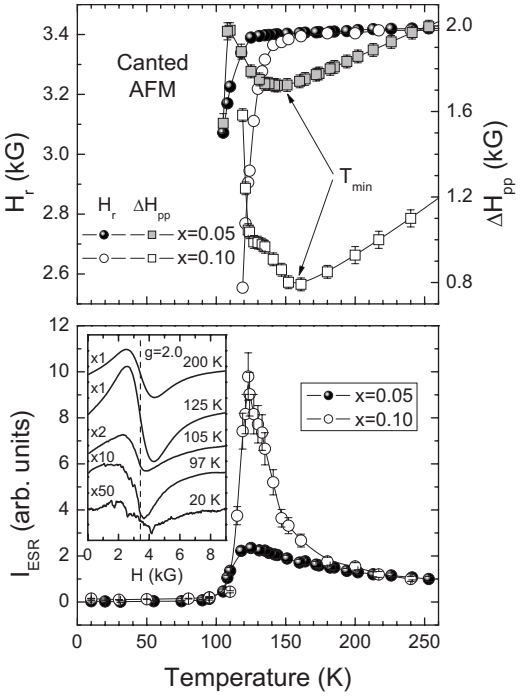

FIG. 2. Temperature dependence of the resonance field H_r, peak-to-peak linewidth ΔH_{pp}, and ESR intensity I_{ESR} for $x=0.05$ and 0.10. The inset in the lower panel shows the temperature dependence of the ESR spectra for $x=0.05$.

$S_1(Mn^{+3})=3/2$, $S_2(Mn^{+4})=2$, and $g=2.0$ and the measured dc susceptibility χ at RT [Fig. 1(a)]. Figure 1(a) shows the corresponding x dependence of $\Delta H_0=\Delta H_{pp}\chi/\chi_0$, which reveals a much slower decrease with x than the bare $\Delta H_{pp}(x)$. This indicates that most of the doping dependence of ΔH_{pp} arises from the decrease of the χ_0/χ brought up by the strong increase of the dc susceptibility with x, a consequence of the strengthening of the DE interaction, as the FMM phase is approached. On the other hand, the slow reduction of $\Delta H_0(x)$ shows no pronounced effect of the DE mechanism, consistent with Huber's theoretical analysis of the infinite-temperature ESR linewidth of $La_{1-x}Ca_xMnO_3$.[54] In that case, the DE interaction has been suggested to cause relatively slow charge motion that does not influence spin dynamics at the time scale of 10^{-13} characterizing the decay of the correlation function in the ESR linewidth.

Previous ESR studies of $LaMnO_{3+\delta}$ have shown that the antisymmetric exchange remains constant through the JT transition, indicating that its origin is mainly due to the tilting of the MnO_6 octahedra,[53,54] which does not vary appreciably with doping. The gradual reduction of $\Delta H_0(x)$ can then be related to the weakening of the cooperative JT distortion and the release of crystal strain leading to the decrease of the CF contribution. This effect is depicted in the inset of Fig. 1(b), which shows the decrease of the orthorhombic strain $s=2(a-c)/(a+c)$ with x, calculated from the structural data of the $La_{1-x}Ca_xMnO_3$ samples at RT.[31] Recent neutron-scattering experiments have shown that this structural variation is accompanied by a decrease of the SE coupling anisotropy, as x increases toward the FMM phase.[39] The latter effect leads to an increase of the average SE coupling constant function $\langle J^2\rangle=(2J_{ac}^2+J_b^2)/3$ entering the fourth spectral moment[54] that would also promote exchange narrowing of the ESR line with x. Moreover, no pronounced change of ΔH_0 is observed at $x \geqslant 0.15$, where the Jahn-Teller transition line intersects RT [$T_{JT}(x) < 300$ K]. On the other hand, previous ESR results for lightly doped $LaMnO_3$ have shown that the JT transition to the pseudocubic O^* phase and the accompanying decrease of the CF interaction reduce drastically ΔH_0.[53,55,56] The small decrease of ΔH_0 observed for the present samples at $x \geqslant 0.15$ suggests then a reduction of the JT distortion near the metallic phase, which would depress any significant narrowing of the ESR line. Furthermore, a nonmonotonous variation of ΔH_0 is observed at the CAF-FMI boundary ($x=0.125$), which may be associated with the concomitant reduction of crystal symmetry from orthorhombic $O^/$ to monoclinic $M^/$,[34] and the canceling of the AFM SE interplane coupling ($J_b=0$).[27]

A. CAF phase ($0 < x < 0.125$)

Figure 2 summarizes the temperature dependence of the resonance field H_r, peak-to-peak linewidth ΔH_{pp}, and the integrated ESR intensity I_{ESR} for $x=0.05$ and 0.10, where magnetic measurements have shown a transition to the CAF state at $T_N \approx 130$ K.[31] Both compounds exhibit a quasilinear de-

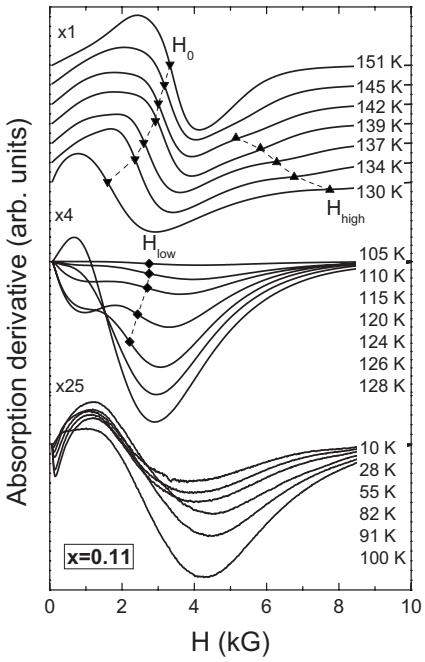

FIG. 3. Temperature dependence of the ESR spectra for $La_{0.89}Ca_{0.11}MnO_3$ at the X band (ν=9.41 GHz).

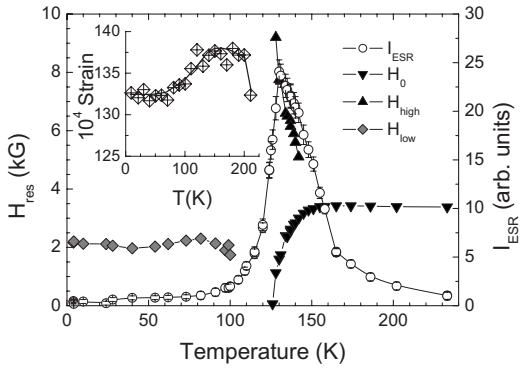

FIG. 4. Temperature dependence of the resonance fields and ESR intensity I_{ESR} for x=0.11. The inset shows the temperature dependence of the orthorhombic strain parameter $s=2(a-c)/(a+c)$ for x=0.11.

crease of ΔH_{pp} down to a minimum value at $T_{min} \approx 150$ and 160 K for x=0.05 and 0.10, respectively. At $T < T_{min}$, ΔH_{pp} increases rapidly toward T_N, in agreement with the linewidth broadening that was previously observed near the AFM transition in lightly doped $LaMnO_3$.[53–55] The ESR intensity reaches a maximum around T_N, while the resonance field shifts rapidly to lower fields for both compounds. The variation of the ESR parameters is more pronounced for x=0.10, reflecting the increase of the mean canting angle and the growth of the FM spin component in the CAF structure at this doping range.[27] Although I_{ESR} does not disappear immediately below T_N, a trace of a broad FM-like signal can be discerned at low temperatures (inset of Fig. 2). The corresponding resonance intensity amounts to $\lesssim 1\%$ of the maximum $I_{ESR}(T)$ for both compounds, indicating that the concentration of any separate FM regions coexisting with the CAF matrix at $x \leqslant 0.10$ is rather small.

Figure 3 shows the temperature dependence of the ESR spectra for x=0.11, which differs considerably from the ordinary AFM behavior. In the PM region, a single ESR line is observed at H_0, which shifts continuously to low fields at $T < 150$ K, accompanied by significant line-shape distortion, including a small kink at H_{high} that shifts toward higher fields. At $T < 125$ K, the resonance line splits into two components, one that evolves from the main resonance and shifts rapidly to zero field, while a minor component is disclosed at $H_{low} \approx 2$ kG, which persists down to low temperatures. Figure 4 shows the corresponding temperature dependence of the resonance fields and ESR intensity for x=0.11. The intensity I_{ESR} increases significantly upon cooling followed by a sharp drop at $T < 130$ K, while in the same T range, the main resonance at H_0 shifts toward zero field. This temperature variation resembles that of the uniform FMR mode appearing below T_C in polycrystalline ferromagnets. In that case, the growth of magnetic anisotropy results in the shift of the resonance line, while recent FMR simulations have shown that it also leads to an increase of the resonance intensity as the anisotropy field approaches $H_0 = \omega/\gamma$.[57] Magnetic measurements have shown that the real part of the ac susceptibility for the x=0.11 sample exhibits a double peak structure, a shoulder at $T \approx 135$ K followed by a sharper peak at $T \approx 120$ K indicative of two successive magnetic transitions, FM at higher T and AFM at lower T.[31] Neutron diffraction has shown that the ground state is the canted AFM with a large FM spin component along the b axis and a canting angle of the magnetic moment from the ac plane of $\approx 48°$ (*Pnma* notation), which evolves directly from the canting of the layered A-AFM spin structure of $LaMnO_3$.[34] Similar behavior with T_{FM} in the range of 130–138 K and $T_{AFM} \approx 112$ K has been previously observed by neutron-diffraction and magnetic measurements for single crystals with x=0.1.[27,49,58] The pronounced shift of H_0 and the fast increase of I_{ESR} can be accordingly explained by the approach to the FM transition and the subsequent increase of the local anisotropy field in the FM phase. As magnetic anisotropy continues to grow upon cooling, it causes the shift of spectral weight out of the X-band field range leading, along with development of AFM order at lower temperatures, to the wipe out of the resonance intensity. Recently, a comparative ESR study of crushed micron sized single crystals and a powder of nanometer sized crystals with x=0.1 in the temperature range of $115 \leqslant T \leqslant 600$ K has shown a similar variation to the present data for the former specimens, whereas FM behavior was inferred for the nanocrystals' cores.[59] This difference was attributed to the compositional gradients of the Ca content in $La_{1-x}Ca_xMnO_3$ single crystals grown by the floating zone method and the presence of local strains.[60] These structural imperfections have been suggested to vary the spatial distribution of the DE interaction leading to mesoscopic phase fluctuations that effectively shift the transition to the FM state at higher doping levels,[58] and may also rationalize the differences between ceramic and single-crystal data in the CAF regime.

On the other hand, the broad low-field line at H_{low} remains clearly resolved down to low temperatures (Fig. 3), with weak but appreciable intensity, which is considerably

larger than that observed for the $x=0.05$ and 0.10 samples. The presence of such resonance mode suggests a separate FM component of low magnetic anisotropy. Its origin may be associated with the hole-rich FM clusters identified by neutron scattering at $x \leqslant 0.1$,[25,27,28] provided that their coupling with the CAF matrix is weak enough to allow the observation of a separate resonance line. In the CAF state, these FM inhomogeneities have been found to be nanosized FM platelets confined mostly within the *ac* plane and strongly coupled with the surrounding AFM matrix, with little size variation as x increases up to the CAF-FMI boundary, above which they start to percolate. However, a similar FM resonance is systematically detected in the FMI phase of the present samples up to $x=0.16$, as will be shown below. This implies that the observed FM signal may be related to a low concentration of residual FM domains of weak anisotropy, most pronounced at $x>0.1$, where ferromagnetism sets out. The formation of such FM inhomogeneities could be triggered by the large crystal strain that develops at $T<T_{JT}$. In particular, the average crystal strain in the JT distorted phase (O' or M') of $La_{1-x}Ca_xMnO_3$ reaches a maximum at the magnetic transition, below which it decreases down to the low-T structural transformation at $T_{M'M''}$, where a marked reduction of the average orthorhombicity occurs, especially in the FMI phase ($x \geqslant 0.125$). The inset of Fig. 4 shows the temperature variation of the orthorhombic strain $s=2(a-c)/(a+c)$ calculated from the structural data of the $x=0.11$ sample.[34] Despite its relatively weak temperature dependence, a continuous release of the average crystal strain is observed down to $T \approx 100$ K, while at lower temperatures, s reaches a nearly constant value, correlating with the appearance of the low-field FMR line.

B. FMI phase ($0.125 \leqslant x \leqslant 0.19$)

Figure 5 (upper panel) shows the temperature dependence of the magnetic-resonance spectra for $x=0.16$, which shows a transition to the FMI state at $T_C \approx 180$ K. A single exchange narrowed ESR line is observed in the PM regime. At $T \leqslant T_C$, the resonance spectrum evolves to a double-line pattern consisting of a low-field peak and a derivative like line at resonance fields designated by H_{1p} and H_{2p}, respectively. These two singularities split continuously as temperature decreases down to ≈ 150 K, following approximately the relation $|H_{1p}-H_0| \simeq 2(H_{2p}-H_0)$, where $H_0 \simeq 3.36$ kG at the microwave frequency $\nu \approx 9.41$ GHz. This asymmetrical spectrum is characteristic of the FMR line shape in polycrystalline ferromagnets with uniaxial magnetic anisotropy energy (MAE).[57,61,62] In the case of a positive anisotropy field $H_a=2K_u/M$, where K_u is the uniaxial anisotropy constant, and weak anisotropy $H_a \ll H_0$, the first derivative FMR powder spectrum determined by the imaginary part of the scalar susceptibility averaged over all orientations of H_a with respect to the applied magnetic field[61] shows two well defined singularities, a relatively weaker absorptionlike peak at low fields $H_{r\|}=H_0-H_a$ (particles with their easy axis along H) and a derivativelike line at higher fields $H_{r\perp}=H_0+H_a/2$ (particles with their easy axis perpendicular to H) satisfying the relation $|H_{r\|}-H_0|=2(H_{r\perp}-H_0) \approx H_a$, whereas the reversed pattern is predicted for $H_a<0$.[62]

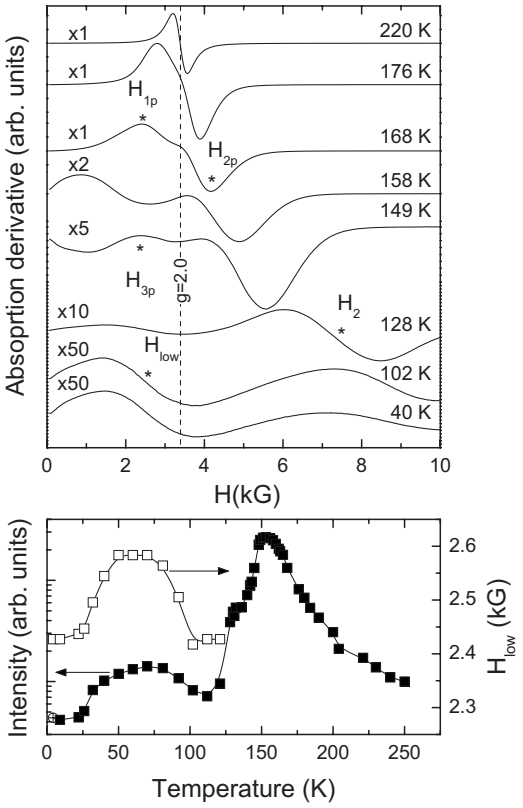

FIG. 5. (Upper panel) Temperature dependence of the magnetic-resonance spectra for $La_{0.84}Ca_{0.16}MnO_3$ at the X band ($\nu = 9.41$ GHz). (Lower panel) Temperature variation of the resonance intensity $I(T)$ in logarithmic scale and $H_{low}(T)$ in an expanded field scale.

This type of spectral asymmetry corresponds exactly to the observed FMR line shape down to $T \approx 150$ K, where H_{1p} and H_{2p} can be assigned to $H_{r\|}$ and $H_{r\perp}$, leading to the peak-to-peak linewidth $\Delta H_{pp}=H_{r\perp}-H_{r\|} \approx 3H_a/2$ that increases upon cooling due to the increment of H_a. At $T<150$ K, the increase of the anisotropy field that becomes $H_a \sim H_0$ shifts the low-field peak to zero field, turning the corresponding absorption to nonresonant. In this case, the quadratic resonance condition for uniaxial MAE yields two resonance modes, when the magnetic field is applied perpendicular to the easy axis.[63] These two lines occur at resonance fields almost symmetrically displaced around H_a, and shift to higher fields as H_a continues to increase.[57] This temperature variation is indeed observed in the FMR spectra at $T<150$ K, where $H_{r\perp}$ splits into two broad lines that merge gradually into one at H_2, which subsequently shifts toward high magnetic fields. However, a broad line of weak intensity, similar to that of the $x=0.11$ sample, appears at low magnetic fields (H_{low}) at $T \lesssim 130$ K, as the high-field mode (H_2) of the uniaxial FMR spectra shifts out of the magnetic-field range. The resonant intensity $I(T)$, derived by double integration of the derivative spectra (lower panel of Fig. 5), rises from above T_C followed by a sharp decrease below 150 K, where the low-field peak at H_{1p} crosses zero field. This causes the loss of spectral weight out of the integrated magnetic-field range, in agreement with recent FMR simulations showing a maximum of $I(T)$ when $H_a \lesssim \omega/\gamma$.[57] On the

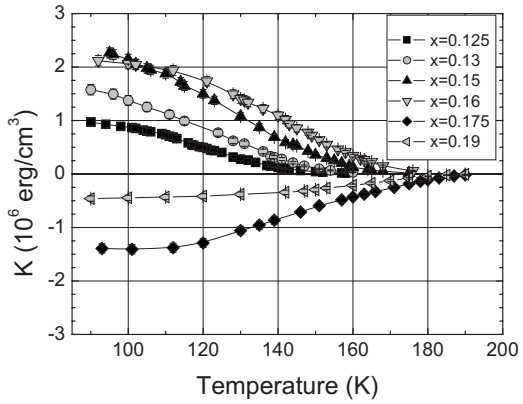

FIG. 6. Temperature dependence of the magnetic anisotropy constant $K(T)$ for various x concentrations in the FMI regime of $La_{1-x}Ca_xMnO_3$. Solid lines through the experimental points are guides to the eyes.

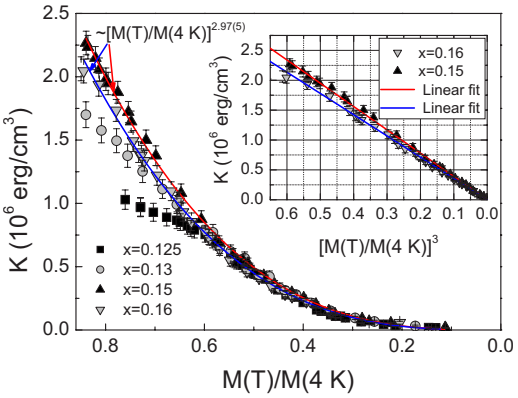

FIG. 7. (Color online) Magnetic anisotropy $K(T)$ as a function of the normalized magnetization $M(T)/M(4\ \mathrm{K})$ for $x=0.125-0.16$. Solid lines show the power-law fits with a best-fit exponent $m=2.97(5)$ for $x=0.15$ and 0.16. The inset shows K vs $[M(T)/M(4\ \mathrm{K})]^3$ plots for $x=0.15$ and 0.16 following a linear variation.

other hand, a broad peak of $I(T)$ is observed simultaneously with $H_{\mathrm{low}}(T)$ at $T\approx 70$ K, where the low-field FMR mode is dominant in the FMR spectra. This peak occurs at the $T_{M/M//}$ transition line [Fig. 1(b)], indicating the close relation of the weak anisotropy FMR mode with the crystal strain.

Qualitatively, similar FMR spectra of uniaxial anisotropy have been observed in the FMI regime with Ca concentrations $0.125\leqslant x\leqslant 0.16$. The main difference with $x=0.16$ is the temperature variation of the high-field H_2 component at $T<110$ K mainly for $x=0.125$,[45] and to a lesser extent for $x=0.13$, which show a more complex behavior that is most likely associated with the presence of a small A-AFM spin component in the neutron diffraction patterns of these samples.[34] At $x=0.175$, a three-mode FMR spectrum is observed, which has been attributed to a change toward negative cubiclike MAE, where three singularities along the [100], [110], and [111] cubic axes are expected in the weak anisotropy limit ($|H_a|\ll H_0$).[45] An asymmetric FMR spectrum with no clearly resolved structure is further observed at $x=0.19$, which, however, preserves the characteristic asymmetry of the FMR line shape for cubic polycrystalline ferromagnets,[64] with considerably reduced H_a. It should be noted that an alternative explanation based on the presence of two separate FM spin systems has been put forward to explain the three-line FMR spectra observed at $T>100$ K in loose packed samples of sizable crystallites (5–20 μm) with $x=0.18$ and 0.20,[40,65] which, however, were subject to partial orientation and demagnetizing effects.

The doping variation of the FMR line shape points to an increase of the anisotropy field for $0.125\leqslant x\leqslant 0.175$, which decreases rapidly as x tends to the metallic phase. To estimate quantitatively the anisotropy constant $K(x,T)$ as a function of doping and temperature, we have employed the temperature variation of $H_a=2K/M$ and of the magnetization M.[34] For $0.125\leqslant x\leqslant 0.16$, $H_a(x,T)$ has been calculated by the total width of the uniaxial FMR spectra as $H_a\approx 2\Delta H_{\mathrm{pp}}/3$, down to temperatures, where all the components of the FMR powder patterns are observable, while at lower temperatures, the resonance position of the high-field component at $H_2\approx H_a$ has been used. To obtain a more complete picture of the $K(x,T)$ evolution, we have extended this calculation to $x=0.175$ and 0.19, relying on the presence of cubiclike MAE. For these concentrations, the anisotropy field has been determined from $H_a\approx 3\Delta H_{\mathrm{pp}}/5$ down to temperatures, where the three-line FMR spectrum is observed, while at lower temperatures, we have exploited the high-field component, which in this case can be assigned to $H_{[100]}=H_0-H_a$ that is least affected by higher-order anisotropy terms.[64] For all samples, $H_a(x,T)$ has been calculated down to $T\approx 90$ K, which is higher than the $T_{M'M''}$ transition line (Fig. 1), where higher-field experiments would be needed to resolve the FMR spectra variation.

Figure 6 shows the resulting $K(T)$ curves as a function of x in the FMI regime. A continuous increase of $K(T)$ is derived with decreasing temperature at $T<T_C$, which reaches 2×10^6 erg/cm^3 at 100 K for $x=0.15$ and 0.16, followed by a drastic reduction for $x=0.19$. Such a pronounced $K(T)$ variation resembles the power-law T dependence expected for single-ion magnetocrystalline anisotropy.[66,67] In particular, the temperature dependence of MAE determined by the interplay of spin-orbit coupling and CF interaction is considered to have the same origin as that of the magnetization, resulting in the power-law variation $K(T)/K(0)\propto[M(T)/M(0)]^{l(l+1)/2}$, where l is the order of the spherical harmonic that describes the angular dependence of the local anisotropy.[66,67] For a uniaxial system, where $l=2$, the corresponding $m=l(l+1)/2$ exponent becomes $m=3$, while at temperatures close to T_C, an $l(l+1)=2$ exponent is predicted.

Figure 7 shows plots of $K(T)$ as a function of the normalized magnetization $M(T)/M(4\ \mathrm{K})$ for $x=0.125-0.16$, where uniaxial magnetic anisotropy has been deduced from the FMR spectra. Fits of the experimental data to a power-law dependence of the form $K\propto[M(T)/M(4\ \mathrm{K})]^m$ lead to an exponent $m=2.97(5)$ for $x=0.15$ and 0.16 over the entire temperature range. This value is very close to the $m=3$ exponent expected for uniaxial single-ion MAE. This is further depicted in the inset of Fig. 7, which shows plots of K vs $[M(T)/M(4\ \mathrm{K})]^3$ that scale linearly for both $x=0.15$ and

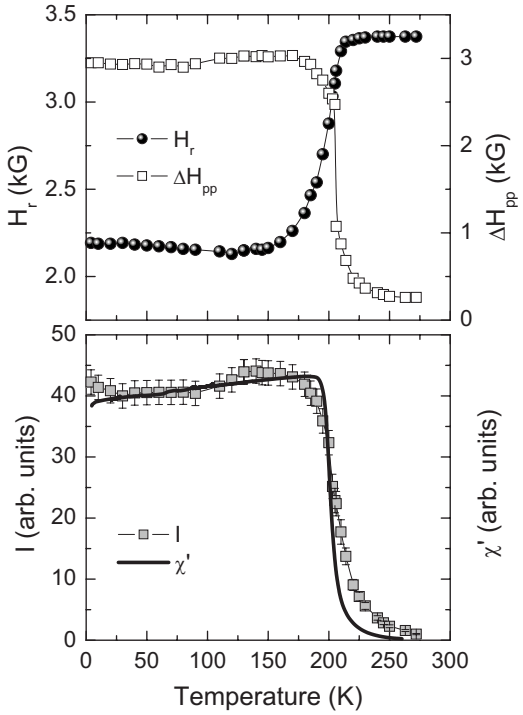

FIG. 8. (Upper panel) Temperature dependence of the resonance field H_r and peak-to-peak linewidth ΔH_{pp} for $x=0.22$. (Lower panel) Temperature dependence of the resonant intensity $I(T)$ compared to the real part of the ac susceptibility $\chi'(T)$.

0.16. On the other hand, a progressive deviation from the $m=3$ power law is observed for $x=0.13$ and 0.125. This variation occurs at $T\lesssim 110$ K and stems directly from the relatively reduced temperature-dependent shift of the high-field H_2 line for these samples. The presence of single-ion MAE with magnitude of 10^6 erg/cm^3 and its close relation to the orientation of the manganese e_g orbitals[1,17] point to a dominant orbitally ordered phase within the FMI regime, with MAE that weakens appreciably as x increases toward the FMM phase. Comparison with the magnetic anisotropy derived from FMR or torque magnetometry for $La_{1-x}Sr_xMnO_3$ compounds as well as CMR manganites near optimal doping ($x=1/3$) in single crystal or thin-film form[68–71] shows that apart from shape anisotropy, MAE is markedly reduced (over an order of magnitude) for those compounds, reflecting mostly the enhanced e_g one-electron bandwidth for the Sr-doped manganites and the suppression of lattice distortions for the metallic phase at $x=1/3$. Even higher MAE would be accordingly anticipated by the enhanced JT distortion for narrow bandwidth manganites, as indeed found for the magnetic anisotropy in the FMI state of $Pr_{0.8}Ca_{0.2}MnO_3$ single crystals.[72]

C. FMI-FMM phase boundary ($0.19\leqslant x\leqslant 0.23$)

For $x=0.22$ and 0.23 residing in the verge of the FMI-FMM phase transition, a single FMR line with no apparent structure is observed below T_C. Figure 8 summarizes the temperature dependence of H_r and ΔH_{pp} for $x=0.22$, which vary weakly below T_C down to low temperatures with a shal-

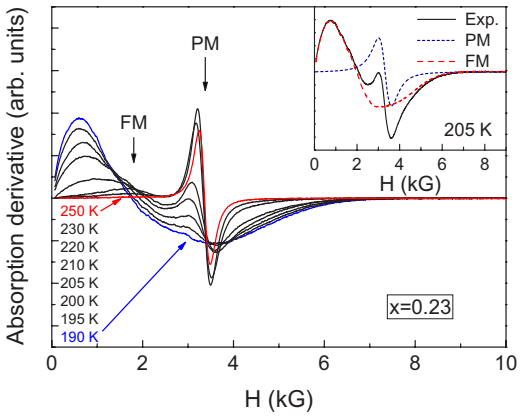

FIG. 9. (Color online) Temperature variation of the magnetic-resonance spectra for $La_{0.77}Ca_{0.23}MnO_3$ at the X band ($\nu=9.41$ GHz). The inset depicts the spectral decomposition into a PM and an FM resonance line at 205 K.

low change at $T\simeq 100$ K, reminiscent of the $T_{M'M''}$ structural transformation. Likewise, the resonance intensity $I(T)$ shows little T dependence at $T<T_C$ and follows closely the real part of the ac susceptibility $\chi'(T)$ (lower panel of Fig. 8). This behavior is characteristic of a soft polycrystalline FM material and verifies the reduction of MAE near the metallic phase boundary. On the other hand, the formation of a small concentration of FM inhomogeneities has been traced in the PM regime for $x=0.175$ and 0.19.[45] This effect appears much more pronounced for the samples with $x=0.22$ and 0.23, straddling the FMI-FMM transition. Figure 9 shows representative ESR spectra for $x=0.23$. In this case, a low-field FMR mode emerges gradually at $T<260$ K, coexisting with the PM resonance line at $g\approx 2.0$. As the temperature decreases toward T_C, the spectral intensity is continuously transferred from the PM to the FMR line until the PM resonance is diminished. To extract the relative spectral weight of each component, we have fitted the central PM line to a Lorentz line shape over the appropriate magnetic-field range around $g\approx 2.0$ plus a polynomial background to account for the FMR contribution. Subsequently, the fitted PM line has been subtracted from the total ESR spectrum to derive the FMR component, as shown in the inset of Fig. 9. This procedure resulted in a fairly accurate decomposition of the ESR spectra, especially for loose packed powder samples, where the FMR line narrows and shifts to lower magnetic field due to partial orientation effects that effectively increase the splitting of the two signals.[50]

Figure 10 shows the resulting temperature variation of the integrated intensity of the FMR component normalized to the total resonant intensity $I_{FM}^{norm}=I_{FM}/(I_{FM}+I_{PM})$ for $x=0.19$, 0.22, and 0.23. The relative FM intensity $I_{FM}^{norm}(T)$ grows considerably with x implying an increase of the underlying FM fraction and shows a rapid increase upon lowering temperature through T_C. This (x,T) evolution of I_{FM}^{norm} correlates with the enhancement of the metallic behavior below T_C, depicted by the corresponding resistivity curves $\rho(T)/\rho(300\text{ K})$ in the inset of Fig. 10. Moreover, the FM phase appears for all samples at the same temperature of $T\approx 260$ K, which lies close to the $T_{JT}(x)$ transition line, when extrapolated at

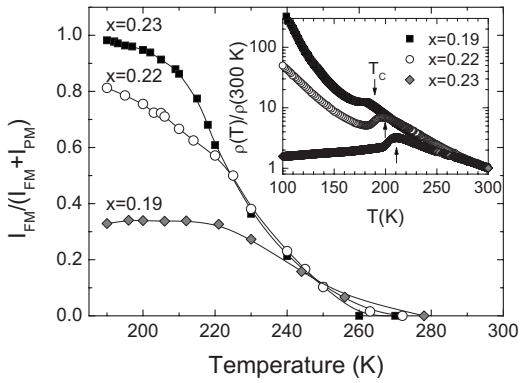

FIG. 10. Temperature variation of the normalized FM intensity $I_{\mathrm{FM}}^{norm}=I_{\mathrm{FM}}/(I_{\mathrm{FM}}+I_{\mathrm{PM}})$ for $x=0.19$, 0.22, and 0.23. The inset shows the corresponding temperature dependence of the normalized resistivity $\rho(T)/\rho(300\ \mathrm{K})$.

higher x values [Fig. 1(b)]. This variation complies with recent ESR results on a ceramic $La_{0.75}Ca_{0.25}MnO_3$ sample[73] as well as $La_{1-x}Sr_xMnO_3$ single crystals in the FMI regime,[74] where the presence of FMR signals in an extended temperature range above T_C has been observed. On the other hand, the coexistence of FMR and PM signals at $T>T_C$ has been reported in a rather limited temperature interval ($\Delta T\approx 3$ K) for a powder ceramic sample with $x=0.33$, attributed to a narrow T_C distribution,[52] while magnetization and NMR experiments on $La_{2/3}Ca_{1/3}MnO_3$ ceramics with different grain sizes have shown a poorly conducting magnetic layer at the grain surface with similar T_C as the bulk one that may account for the low-field magnetoresistance of CMR manganites.[75] Even though the presence of such extrinsic inhomogeneities cannot be completely ruled out, the systematic evolution of the FMR signal with x suggests an intrinsic effect involving the formation of FM clusters above T_C as the FMI-FMM phase boundary is approached. The nucleation of such FM inhomogeneities may be driven by short-range orbital correlations that persist in the metallic phase despite the absence of a cooperative Jahn-Teller transition.[76] Such an effect can be of direct relevance to the heterogeneous electronic phase-separation approach of the CMR effect,[77] as well as to the suppression of a genuine FM phase transition close to the FMI-FMM boundary, which is restored near optimal doping ($x=1/3$).[78]

IV. CONCLUSIONS

In summary, we have performed a systematic ESR study in stoichiometric $La_{1-x}Ca_xMnO_3$ over an extended concentration range ($0<x\leqslant 0.23$) to probe the evolution of spin dynamics and phase coexistence as a function of doping. The room-temperature ESR linewidth decreases significantly with x, a variation that is mainly due to the reduction of the thermodynamic factor $[T\chi(x)]^{-1}$ and to a lesser extent to a much slower evolution of spin relaxation attributed to the interplay of CF and SE interactions with no noticeable signature of the DE mechanism. In the CAF regime ($0<x<0.125$), AFM behavior is observed in the vicinity of T_N preceded by an x-dependent FM variation of the ESR parameters that reflects the growth of the FM spin component in the canted spin structure. A minor contribution from a low-field FMR mode is further observed below T_N that becomes enhanced near the CAF-FMI phase boundary ($x=0.11$). This mode persists at higher doping levels in the FMI phase, up to $x=0.16$, and it is likely related to the release of crystal strain near the low-temperature $T_{M'M''}$ structural transformation that may cause the appearance of residual FM domains with weak magnetic anisotropy. In the FMI regime, FMR measurements reveal uniaxial magnetic anisotropy that reaches 10^6 erg/cm^3 and follows an $M(T)^3$ temperature dependence above $T_{M'M''}$ for $x=0.15$ and 0.16, pointing to the single-ion magnetocrystalline origin of MAE and the presence of an orbitally ordered ferromagnetic insulating state. The magnetic anisotropy decreases significantly as the FMI-FMM phase boundary is approached, where the appearance of an FMR mode coexisting with the PM resonance line is systematically observed at $T\leqslant 260$ K for $x=0.19-0.23$. The relative intensity of that FMR line grows appreciably with x indicating an increase of the underlying FM fraction that correlates with the enhancement of the metallic behavior of the sample's resistivity.

[1] Y. Tokura and N. Nagaosa, Science **288**, 462 (2000).
[2] C. Zener, Phys. Rev. **82**, 403 (1951); P. W. Anderson and H. Hasegawa, *ibid.* **100**, 675 (1955); P. G. de Gennes, *ibid.* **118**, 141 (1960).
[3] M. Imada, A. Fujimori, and Y. Tokura, Rev. Mod. Phys. **70**, 1039 (1998).
[4] J. M. D. Coey, M. Viret, and S. von Molnár, Adv. Phys. **48**, 167 (1999).
[5] Y. Tokura and Y. Tomioka, J. Magn. Magn. Mater. **200**, 1 (1999).
[6] E. Dagotto, T. Hotta, and A. Moreo, Phys. Rep. **344**, 1 (2001).
[7] J. B. Goodenough and J.-S. Zhou, in *Structure and Bonding*, edited by J. B. Goodenough (Springer-Verlag, Berlin, 2001), Vol. 98.
[8] R. Kajimoto, H. Mochizuki, H. Yoshizawa, S. Okamoto, and S. Ishihara, Phys. Rev. B **69**, 054433 (2004).
[9] J. Geck, P. Wochner, S. Kiele, R. Klingeler, A. Revcolevschi, M. v. Zimmermann, B. Buchner, and P. Reutler, New J. Phys. **6**, 152 (2004).
[10] M. Hennion and F. Moussa, New J. Phys. **7**, 84 (2005).
[11] J. Rodriguez-Carvajal, M. Hennion, F. Moussa, A. H. Moudden, L. Pinsard, and A. Revcolevschi, Phys. Rev. B **57**, R3189 (1998).
[12] X. Qiu, Th. Proffen, J. F. Mitchell, and S. J. L. Billinge, Phys. Rev. Lett. **94**, 177203 (2005).
[13] E. Wollan and W. C. Koeller, Phys. Rev. **100**, 545 (1955).
[14] J. B. Goodenough, Phys. Rev. **100**, 564 (1955).
[15] F. Moussa, M. Hennion, J. Rodriguez-Carvajal, H. Moudden, L. Pinsard, and A. Revcolevschi, Phys. Rev. B **54**, 15149 (1996).

[16] D. Khomskii and G. Sawatzky, Solid State Commun. **102**, 87 (1997).
[17] I. Solovyev, N. Hamada, and K. Terakura, Phys. Rev. Lett. **76**, 4825 (1996).
[18] A. J. Millis, Phys. Rev. B **55**, 6405 (1997).
[19] S. Mitsudo, K. Hirano, H. Nojiri, M. Motokawa, K. Hirota, A. Nishizawa, N. Kaneko, and Y. Endoh, J. Magn. Magn. Mater. **177-181**, 877 (1998).
[20] L. Mihály, D. Talbayev, L. F. Kiss, J. Zhou, T. Fehér, and A. Jánossy, Phys. Rev. B **69**, 024414 (2004).
[21] D. Talbayev, L. Mihály, and J. Zhou, Phys. Rev. Lett. **93**, 017202 (2004).
[22] J. Geck, M. Hücker, B. Büchner, R. Gross, L. Pinsard-Gaudart, and A. Revcolevschi, Phys. Rev. B **64**, 144430 (2001).
[23] A. Pimenov, M. Biberacher, D. Ivannikov, A. Loidl, V. Yu. Ivanov, A. A. Mukhin, and A. M. Balbashov, Phys. Rev. B **62**, 5685 (2000).
[24] D. Ivannikov, M. Biberacher, H.-A. Krug von Nidda, A. Pimenov, A. Loidl, A. A. Mukhin, and A. M. Balbashov, Phys. Rev. B **65**, 214422 (2002).
[25] M. Hennion, F. Moussa, G. Biotteau, J. Rodríguez-Carvajal, L. Pinsard, and A. Revcolevschi, Phys. Rev. Lett. **81**, 1957 (1998).
[26] F. Moussa, M. Hennion, G. Biotteau, J. Rodríguez-Carvajal, L. Pinsard, and A. Revcolevschi, Phys. Rev. B **60**, 12299 (1999).
[27] G. Biotteau, M. Hennion, F. Moussa, J. Rodríguez-Carvajal, L. Pinsard, A. Revcolevschi, Y. M. Mukovskii, and D. Shulyatev, Phys. Rev. B **64**, 104421 (2001).
[28] P. Kober-Lehouelleur, F. Moussa, M. Hennion, A. Ivanov, L. Pinsard-Gaudart, and A. Revcolevschi, Phys. Rev. B **70**, 144409 (2004).
[29] P. Schiffer, A. P. Ramirez, W. Bao, and S.-W. Cheong, Phys. Rev. Lett. **75**, 3336 (1995).
[30] T. Okuda, Y. Tomioka, A. Asamitsu, and Y. Tokura, Phys. Rev. B **61**, 8009 (2000).
[31] M. Pissas and G. Papavassiliou, J. Phys.: Condens. Matter **16**, 6527 (2004).
[32] G.-L. Liu, J.-S. Zhou, and J. B. Goodenough, Phys. Rev. B **70**, 224421 (2004).
[33] B. B. Van Aken, O. D. Jurchescu, A. Meetsma, Y. Tomioka, Y. Tokura, and T. T. M. Palstra, Phys. Rev. Lett. **90**, 066403 (2003).
[34] M. Pissas, I. Margiolaki, G. Papavassiliou, D. Stamopoulos, and D. Argyriou, Phys. Rev. B **72**, 064425 (2005).
[35] J. W. Lynn, R. W. Erwin, J. A. Borchers, Q. Huang, A. Santoro, J.-L. Peng, and Z. Y. Li, Phys. Rev. Lett. **76**, 4046 (1996).
[36] P. Dai, J. A. Fernandez-Baca, N. Wakabayashi, E. W. Plummer, Y. Tomioka, and Y. Tokura, Phys. Rev. Lett. **85**, 2553 (2000).
[37] Y. Endoh, K. Hirota, S. Ishihara, S. Okamoto, Y. Murakami, A. Nishizawa, T. Fukuda, H. Kimura, H. Nojiri, K. Kaneko, and S. Maekawa, Phys. Rev. Lett. **82**, 4328 (1999); Y. Yamada, J. Suzuki, K. Oikawa, S. Katano, and J. A. Fernandez-Baca, Phys. Rev. B **62**, 11600 (2000); D. E. Cox, T. Iglesias, E. Moshopoulou, K. Hirota, K. Takahashi, and Y. Endoh, *ibid.* **64**, 024431 (2001); J. Geck, P. Wochner, D. Bruns, B. Büchner, U. Gebhardt, S. Kiele, P. Reutler, and A. Revcolevschi, *ibid.* **69**, 104413 (2003).
[38] M. v. Zimmermann, C. S. Nelson, J. P. Hill, D. Gibbs, M. Blume, D. Casa, B. Keimer, Y. Murakami, C.-C. Kao, C. Venkataraman, T. Gog, Y. Tomioka, and Y. Tokura, Phys. Rev. B **64**, 195133 (2001).
[39] M. Hennion, F. Moussa, P. Lehouelleur, F. Wang, A. Ivanov, Y. M. Mukovskii, and D. Shulyatev, Phys. Rev. Lett. **94**, 057006 (2005).
[40] V. Markovich, E. Rozenberg, A. I. Shames, G. Gorodetsky, I. Fita, K. Suzuki, R. Puzniak, D. A. Shulyatev, and Ya. M. Mukovskii, Phys. Rev. B **65**, 144402 (2002).
[41] V. Markovich, I. Fita, R. Puzniak, M. I. Tsindlekht, A. Wisniewski, and G. Gorodetsky, Phys. Rev. B **66**, 094409 (2002).
[42] V. Markovich, G. Jung, Y. Yuzhelevski, G. Gorodetsky, A. Szewczyk, M. Gutowska, D. A. Shulyatev, and Ya. M. Mukovskii, Phys. Rev. B **70**, 064414 (2004).
[43] G. Papavassiliou, M. Belesi, M. Fardis, and C. Dimitropoulos, Phys. Rev. Lett. **87**, 177204 (2001).
[44] G. Papavassiliou, M. Pissas, M. Belesi, M. Fardis, J. Dolinsek, C. Dimitropoulos, and J. P. Ansermet, Phys. Rev. Lett. **91**, 147205 (2003).
[45] V. Likodimos and M. Pissas, Phys. Rev. B **73**, 214417 (2006).
[46] Q. Huang, A. Santoro, J. W. Lynn, R. W. Erwin, J. A. Borchers, J. L. Peng, K. Ghosh, and R. L. Greene, Phys. Rev. B **58**, 2684 (1998).
[47] B. Dabrowski, R. Dybzinski, Z. Bukowski, O. Chmaissem, and J. D. Jorgensen, J. Solid State Chem. **146**, 448 (1999).
[48] M. Pissas, G. Papavassiliou, E. Devlin, A. Simopoulos, and V. Likodimos, Eur. Phys. J. B **47**, 221 (2005).
[49] B. Martínez, V. Laukhin, J. Fontcuberta, L. Pinsard, and A. Revcolevschi, Phys. Rev. B **66**, 054436 (2002).
[50] A. I. Shames, E. Rozenberg, W. H. McCarroll, M. Greenblatt, and G. Gorodetsky, Phys. Rev. B **64**, 172401 (2001).
[51] A. Abragam and B. Bleaney, *Electron Paramagnetic Resonance of Transition Ions* (Clarendon, Oxford, 1970).
[52] M. T. Causa, M. Tovar, A. Caneiro, F. Prado, G. Ibanez, C. A. Ramos, A. Butera, B. Alascio, X. Obradors, S. Pinol, F. Rivadulla, C. Vázquez-Vázquez, A. López-Quintela, J. Rivas, Y. Tokura, and S. B. Oseroff, Phys. Rev. B **58**, 3233 (1998).
[53] M. Tovar, G. Alejandro, A. Butera, A. Caneiro, M. T. Causa, F. Prado, and R. D. Sánchez, Phys. Rev. B **60**, 10199 (1999).
[54] D. L. Huber, G. Alejandro, A. Caneiro, M. T. Causa, F. Prado, M. Tovar, and S. B. Oseroff, Phys. Rev. B **60**, 12155 (1999).
[55] V. A. Ivanshin, J. Deisenhofer, H.-A. Krug von Nidda, A. Loidl, A. A. Mukhin, A. M. Balbashov, and M. V. Eremin, Phys. Rev. B **61**, 6213 (2000).
[56] J. Deisenhofer, B. I. Kochelaev, E. Shilova, A. M. Balbashov, A. Loidl, and H.-A. Krug von Nidda, Phys. Rev. B **68**, 214427 (2003).
[57] A. Butera, Eur. Phys. J. B **52**, 297 (2006).
[58] E. Rozenberg, G. Jung, M. Auslender, G. Gorodetsky, I. Felner, E. Sominski, A. Gedanken, and Ya. M. Mukovskii, J. Appl. Phys. **99**, 08Q305 (2006).
[59] A. I. Shames, M. Auslender, E. Rozenberg, G. Gorodetsky, E. Sominski, A. Gedanken, and Ya. M. Mukovskii, J. Magn. Magn. Mater. **300**, 12 (2006).
[60] D. Shulyatev, S. Karabashev, A. Arsenov, Ya. Mukovskii, and S. Zverkov, J. Cryst. Growth **237/239**, 810 (2002).
[61] M. Respaud, M. Goiran, F. Yang, J. M. Broto, T. O. Ely, C. Amiens, B. Chaudret, and S. Askenazy, Physica B **246-247**, 580 (1998).
[62] E. de Biasi, C. A. Ramos, and R. D. Zysler, J. Magn. Magn. Mater. **262**, 235 (2003).
[63] M. Farle, Rep. Prog. Phys. **61**, 755 (1998).
[64] D. L. Griscom, J. Magn. Reson. (1969-1992) **45**, 81 (1981); J.

Non-Cryst. Solids **67**, 81 (1984).
[65] A. I. Shames, E. Rozenberg, G. Gorodetsky, and Ya. M. Mukovskii, Phys. Rev. B **68**, 174402 (2003).
[66] H. B. Callen and E. Callen, J. Phys. Chem. Solids **27**, 1271 (1966).
[67] R. Skomski, O. N. Mryasov, J. Zhou, and D. J. Sellmyer, J. Appl. Phys. **99**, 08E916 (2006).
[68] S. E. Lofland, S. M. Bhagat, C. Kwon, S. D. Tyagi, Y. M. Mukovskii, S. G. Karabashev, and A. M. Balbashov, J. Appl. Phys. **81**, 5737 (1997).
[69] Y. Suzuki, H. Y. Hwang, S.-W. Cheong, T. Siegrist, R. B. van Dover, A. Asamitsu, and Y. Tokura, J. Appl. Phys. **83**, 7064 (1998).
[70] V. Dyakonov, V. Shapovalov, E. Zubov, P. Aleshkevych, A. Klimov, V. Varyukhin, V. Pashcenko, V. Kamenev, V. Mikhailov, K. Dyakonov, V. Popov, S. J. Lewandowski, M. Berkowski, R. Zuberek, A. Szewczyk, and H. Szymczak, J. Appl. Phys. **93**, 2100 (2003).
[71] S. Budak, M. Özdemir, and B. Aktas, Physica B **349**, 348 (2004).
[72] V. Markovich, I. Fita, A. I. Shames, R. Puzniak, E. Rozenberg, C. Martin, A. Wisniewski, Y. Yuzhelevskii, A. Wahl, and G. Gorodetsky, Phys. Rev. B **68**, 094428 (2003).
[73] D. L. Cchahuana, E. Winkler, F. Prado, A. Butera, C. A. Ramos, M. T. Causa, and M. Tovar, Physica B **354**, 55 (2004).
[74] J. Deisenhofer, D. Braak, H.-A. Krug von Nidda, J. Hemberger, R. M. Eremina, V. A. Ivanshin, A. M. Balbashov, G. Jug, A. Loidl, T. Kimura, and Y. Tokura, Phys. Rev. Lett. **95**, 257202 (2005).
[75] M. Bibes, Ll. Balcells, J. Fontcuberta, M. Wojcik, S. Nadolski, and E. Jedryka, Appl. Phys. Lett. **82**, 928 (2003).
[76] D. N. Argyriou, J. W. Lynn, R. Osborn, B. Campbell, J. F. Mitchell, U. Ruett, H. N. Bordallo, A. Wildes, and C. D. Ling, Phys. Rev. Lett. **89**, 036401 (2002).
[77] J. Burgy, M. Mayr, V. Martin-Mayor, A. Moreo, and E. Dagotto, Phys. Rev. Lett. **87**, 277202 (2001); M. B. Salamon, P. Lin, and S. H. Chun, *ibid.* **88**, 197203 (2002); J. Burgy, A. Moreo, and E. Dagotto, *ibid.* **92**, 097202 (2004); F. Rivadulla, M. Otero-Leal, A. Espinosa, A. de Andrés, C. Ramos, J. Rivas, and J. B. Goodenough, *ibid.* **96**, 016402 (2006).
[78] C. P. Adams, J. W. Lynn, V. N. Smolyaninova, A. Biswas, R. L. Greene, W. Ratcliff II, S.-W. Cheong, Y. M. Mukovskii, and D. A. Shulyatev, Phys. Rev. B **70**, 134414 (2004); F. Rivadulla, J. Rivas, and J. B. Goodenough, *ibid.* **70**, 172410 (2004).